Detecting Protein Aggregates on Untreated Human Tissue Samples by Atomic Force Microscopy Recognition Imaging

Rhiannon Creasey,[†] Shiwani Sharma,[‡] Jamie E. Craig,[‡] Christopher T. Gibson,[†] Andreas Ebner,[§] Peter Hinterdorfer,[§*] and Nicolas H. Voelcker[†*]

[†]School of Chemical and Physical Sciences, and [‡]School of Medicine, Ophthalmology, Flinders University, Bedford Park, Australia; and [§]Institute for Biophysics, Johannes Kepler Universität Linz, Linz, Austria

ABSTRACT We apply topography and recognition (TREC) imaging to the analysis of whole, untreated human tissue for what we believe to be the first time. Pseudoexfoliation syndrome (PEX), a well-known cause of irreversible blindness worldwide, is characterized by abnormal protein aggregation on the anterior lens capsule of the eye. However, the development of effective therapies has been hampered by a lack of detailed knowledge of the protein constituents in these pathological deposits and their distribution. Using both TREC and immunofluorescence, one of the proteins implicated in the PEX pathology—the apolipoprotein clusterin—was detected, and differences in its distribution pattern on the surface of untreated human lens capsule tissue in both PEX and normal control samples were investigated. Our study shows the potential of TREC imaging for the analysis of whole, untreated human tissue samples.

INTRODUCTION

Atomic force microscopy (AFM) (1) is a versatile surface characterization method, able to provide high-content information on a variety of substrates (2). Samples can be imaged under physiological conditions rendering AFM an ideal technique for high-resolution characterization of biological samples in terms of their topography and, independently, their affinity toward different chemical or biological species immobilized on the AFM tip (3,4). Traditionally, AFM has been unable to combine topography mapping and molecular recognition mapping because the topography could not be separated reliably from binding events between the probe and the surface. However, a modification of the AFM technique has been developed for rapid mapping of receptor binding sites of biological substrates using simultaneous topography and recognition (TREC) imaging (5–10).

TREC operation relies on a receptor-functionalized tip on a magnetic-coated cantilever driven by a magnetic field (MAC mode). In this technique (6,10), the probe amplitude is split into lower and upper regions with respect to the probe's resting position. These regions contain information regarding the topography and recognition events image, correspondingly (7). TREC has been successfully applied to many biological systems, such as pure proteins (5,8,11–13), remodeled chromatic structures (15), and protein superstructures (11). More complicated systems that have made use of TREC include imaging erythrocyte membranes to detect cystic fibrosis transmembrane regulators (16), detection of vascular endothelial-cadherin binding sites in microvascular endothelial mouse cells (17), and demonstration of human ergotoxin channel inhibition in embryonic kidney cell cultures (18). However, TREC imaging has not yet been demonstrated on unfixed tissues using functionalized tips (19).

Most biological tissues would require histological preparation, such as fixation, before imaging studies. Ocular tissues such as the human cornea and sclera have been studied by AFM after fixation and mechanical dissociation of collagen fibrils (20). Cataract has also been studied using AFM after extensive sample preparation to homogenize and extract the membrane proteins from the lens (21). However, as the ocular lens capsule is a relatively smooth (roughness $<$50 nm root mean-square) and thin (20–60 μm (22)) tissue, we conjectured that it might be amenable for direct AFM imaging without fixation. It is a clear membrane encapsulating the ocular lens and is mainly comprised of proteins in the collagen family. Human lens capsule can undergo pathological changes, which manifest in protein misfolding, resulting in protein aggregation. This aggregation is characteristic of Pseudoexfoliation syndrome (PEX) (23), which is caused by the formation of insoluble protein aggregates in the anterior segment of the eye and is characterized by deposition of fibrillar proteinaceous material on the anterior lens capsule (24). One of the main secondary effects of PEX is blockage of the aqueous outflow mechanism of the eye (25). This can lead to elevation of intraocular pressure causing loss of vision due to glaucomatous damage to the optic nerve, the second leading cause of irreversible blindness worldwide (26–28). Currently, treatment methods are limited to those that alleviate intraocular pressure associated with glaucoma, but there is no understanding of how to deal with the underlying PEX protein aggregation (29).

Many factors limit the study of PEX using conventional techniques: there are very small (submicrogram) amounts of material for analysis (30) and the deposits are not readily

Submitted February 13, 2010, and accepted for publication June 18, 2010.

*Correspondence: Nico.Voelcker@flinders.edu.au or Peter.Hinterdorfer@jku.at

Editor: Levi A. Gheber.

0006-3495/10/09/1660/8 $2.00

doi: 10.1016/j.bpj.2010.06.044

soluble (26), confounding analysis. Hence the current knowledge of the protein constituents of PEX deposits is limited. Presence of some protein constituents has been demonstrated by immunohistochemistry and, more recently, by direct mass spectrometry of PEX lens capsule or isolated PEX material (26,27). These analyses have shown the presence of apolipoproteins (26,27,31–33), inflammatory (26), and extracellular matrix proteins (24,26,37) in pathological PEX deposits. Common genetic variants in the *LOXL1* gene, involved in the formation of elastic fibers in the extracellular material (28,34), are associated genetically with PEX (34–36), and LOXL1 protein is present in PEX material (27). Despite this knowledge, the disease mechanism remains poorly understood (35,38). Because of limitations in resolution and environmental control for established antibody recognition techniques, such as immunofluorescence and immuno gold labeling SEM, the protein aggregates themselves cannot be analyzed in their native environment using these techniques. Hence we considered TREC imaging as a suitable technique for this purpose because it can be used to localize proteins in PEX material deposited on lens capsule tissue by imaging the fibrillar deposits at a higher resolution than optically possible, in a physiological environment, and affording topographical information at the same time.

The aim of this study was to apply TREC to whole untreated human tissue. We focused on the apolipoprotein clusterin on the lens capsule, which is known to be present and involved in PEX (26,27,31,33). We first examined binding of clusterin to anti-clusterin antibody by AFM force spectroscopy. Human lens capsules were then imaged using in-fluid AFM, followed by TREC imaging using anti-clusterin antibody functionalized AFM tips. Clusterin was observed on the normal lens capsule surface in small, localized spots whereas the PEX lens capsules showed significantly larger, localized patches of clusterin. These results were confirmed by immunofluorescence imaging. We postulate that the TREC imaging technique, applied with antibodies specific to other known or putative constituents of PEX deposits will lead to a more complete understanding of the disease pathology. Such understanding may form the basis of earlier detection methods and treatments that directly target protein accumulation instead of the subsequent glaucoma and therefore prevent loss of vision or blindness in the affected patients. TREC imaging may also be applicable to other types of tissues such as blood vessels or the retina.

MATERIALS AND METHODS

AFM tip modification

AFM probes were functionalized with anti-clusterin antibodies as described for other antibodies (39). Briefly, AFM probes were amino-functionalized with 3-aminopropyl triethoxysilane (Sigma-Aldrich, St. Louis, MO) using a vapor phase deposition method (40). The heterobifunctional cross-linker NHS-PEG_{800}-aldehyde (prepared as per Ebner et al. (39)) was covalently bound to the amine groups on the tips for 2 h at a concentration on 6.6 mg/mL in chloroform with 1% (vol/vol) triethylamine. After washing and drying, the probes were then immersed in phosphate buffered saline buffer (PBS; 150 mM NaCl, 5 mM NaH_2PO_4, pH 7.4) containing 0.2 mg/mL of HPLC-purified anti-clusterin antibodies (rabbit anti-CLU primary antibody; Santa Cruz Biotechnology, Heidelberg, Germany) and 2 μL of sodium cyanoborohydride ($NaCNBH_3$) solution (32 mg $NaCNBH_3$, 50 μL of 100 mM sodium hydroxide in 450 μL MilliQ water) for 2 h. Subsequently, 5 μL of 1 M ethanolamine-hydrochloride (Sigma-Aldrich) was added to the solution for 10 min to quench any remaining aldehyde groups. Finally, the probes were washed and stored in PBS buffer at 4°C for no more than 1 week.

Sample preparation for AFM

For force spectroscopy measurements, freshly cleaved mica was incubated with recombinant human clusterin (human recombinant clusterin; Biomedica Medizinprodukte, Austria; 150 μg/mL in PBS buffer) for 1 h, and then rinsed 50 times in 500 μL PBS buffer to remove any loose protein. Freshly prepared clusterin samples were placed into the AFM liquid cell and 600 μL PBS buffer was added.

Human lens capsules were collected from patients undergoing cataract surgery, according to the ethical guidelines of the Flinders Clinical Research Ethics Committee, Flinders Medical Centre, Australia. Samples were stored in sterile MilliQ water or balanced salt solution (NaCl, KCl, $CaCl_2 \times H_2O$, $MgCl_2 \times 6H_2O$, $C2H_3NaO_2 \times 3H_2O$, and $C_6H_5Na_3O_7 \times 2H_2O$) at 4°C until use. Lens capsules were carefully washed three times in 1 mL MilliQ water and placed flat on a cleaned glass coverslip. The slide was dried thoroughly under a gentle stream of nitrogen to immobilize the tissue and then rehydrated in the AFM liquid cell with 600 μL PBS buffer. Interestingly, the tissue lifted off the surface if dried from PBS buffer and hence the tissue needed to be either stored in fluid or washed thoroughly with MilliQ water before dry storage. Lens capsules were stable for reuse when stored carefully in PBS buffer at 4°C for up to 1 week. As the AFM experiments were conducted in a nonsterile environment, lens capsules were discarded after 1 week.

AFM

AFM probes (nominal spring constant 0.03 N/m; MSNL; Veeco, Plainview, NY) modified with antibody as described above were used for force spectroscopy measurements as detailed by Riener et al. (41). Briefly, for each functionalized tip prepared, 1000 force spectroscopy curves at a given force loading rate were collected on a Pico-SPM AFM (Molecular Imaging, Santa Clara, CA) using a fluid cell. MATLAB 7.1 (The MathWorks, Natick, MA) was used for force curve analysis and spring constant determination as described by Riener et al. (41). Spring constants were determined using both the Sader (42) and the thermal noise (43,44) methods for Veeco probes, and were found to be between 0.013 and 0.090 N/m.

For AFM topography and recognition measurements, MAC probes (Agilent MACLevers Type VI (N9865B); Agilent Technologies, Santa Clara, CA) with nominal spring constant 0.292 N/m) modified with antibody as above were used for imaging. MAC mode images were acquired using a PicoPlus AFM (Agilent Technologies) fitted with a fluid cell in PBS buffer at room temperature using similar experimental conditions as described by Stroh et al. (5) and Ebner et al. (10). TREC measurements were made in regions of interest of less than 5 × 5 μm^2 and at scanning speeds of 1 line/s (or slower) using full amplitude feedback (7). A very low cantilever drive frequency (3–5 kHz) was used for imaging, as cross talk is minimized due to the extra time for topography signal to decay before recognition signal is measured (7). For the MAC mode probes, the thermal noise method was used for calibration and spring constants were found to be between 0.2 and 0.9 N/m.

The process of blocking verifies probe-ligand specificity, as the interaction between the probe receptor and the surface ligand is interrupted to

remove signal. For both force spectroscopy and TREC imaging experiments, blocking of the antibody on the probe was done with free clusterin or blocking of the surface clusterin was done with anti-clusterin antibodies (150 μg/mL) in PBS buffer. Additional recognition blocking was done by amplitude adjustment as described by Preiner et al. (7) for TREC imaging.

Images for Fig. 1 were acquired using a Nanoscope IV Multimode SPM (Veeco) AFM operating in Acoustic AC (AAC) mode. The cantilevers used were OTR8 probes (0.57 and 0.15 N/m nominal spring constant; Veeco). Freeware Gwyddion data analysis (http://gwyddion.net/) and Nanoscope v6 (Veeco) software was used for AFM data and image analysis.

Immunofluorescence

Human lens capsules were collected from patients undergoing cataract surgery according to the ethical guidelines of the Flinders Clinical Research Ethics Committee, Flinders Medical Centre, Australia. Samples were stored in sterile MilliQ water or balance salt solution at 4°C until used. Human lens capsules were carefully cut into pieces and immobilized in wells of cell culture plate using superfine syringe needles. For immunolabeling of the ZO-1 protein, the samples were washed three times in PBS, blocked in 150 μL 5% donkey serum for 15 min, hybridized with 150 μL rabbit anti-ZO-1 primary antibody (1:400 dilution) (Zymed Laboratories) for 1 h, and then with 150 μL Alexa Fluor-488 conjugated goat anti-rabbit IgG secondary antibody (1:1000 dilution) (Molecular Probes) for 1 h. After each incubation the samples were washed three times in PBS. After labeling, the samples were mounting on glass slides in buffered glycerol. Clusterin was similarly labeled with the rabbit anti-CLU primary antibody (1:250 dilution) (Santa Cruz Biotechnology) without blocking the samples with donkey serum. The negative control sample was incubated with 1% donkey serum instead of a primary antibody. Images were taken on a Leica SP5 Confocal Microscope with Leica Application software using the Argon laser (excitation 488 nm, emission 525 nm) in z-plane optical sections of 1-μm intervals.

RESULTS AND DISCUSSION

Force spectroscopy

Clusterin (apolipoprotein J) was selected as a model protein for the testing of this system as it has been clearly implicated in the PEX pathology (26,27,31,33), and both the protein and antibody are readily available commercially. The NHS-PEG$_{800}$-aldehyde cross-linker was chosen because it allows easy and stable binding of (lysine containing) proteins to amino functionalized tips. This cross-linker has also been used previously for antibody experiments (39), and we have followed the published protocol.

To verify the specificity of the antibody-protein interaction, force spectroscopy was carried out using recombinant human clusterin adsorbed on mica and an anti-clusterin coated AFM tip. Pull-off forces were between 12 and 85 pN with an average unbinding force of 40 pN. These values are slightly lower than other reported antibody-antigen forces (45). However, they are within experimental variation. After incubation of the tip with clusterin to block the antibody, the number of unbinding events dropped from 7% to 2% at 300 nm/s tip velocity, indicating that the adhesion is occurring primarily due to the antibody-protein interaction, and validating the specificity of the modified probe. Force spectroscopy can also be used to determine the stretched linker length before unbinding. The average linker length was calculated as 20 nm ($\pm$4 nm), which is expected as the theoretical length of the linker combined with an antibody is 20 nm (5). This information from the force spectroscopy data is useful for calculation of amplitudes necessary for TREC data collection.

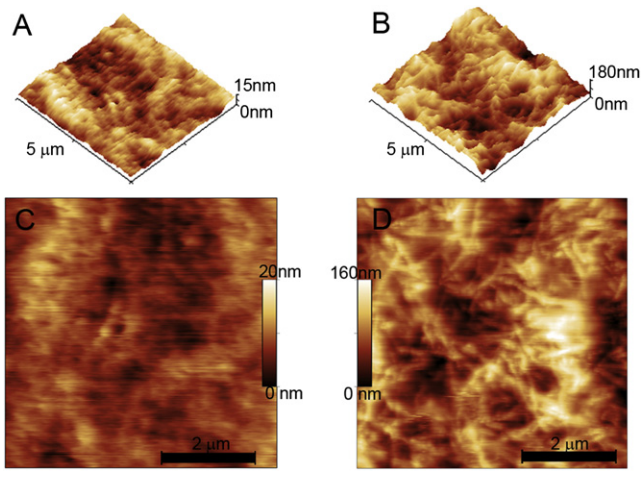

FIGURE 1 (*A*) Three-dimensional representation of an AFM image of normal lens capsule on glass using AAC mode in MilliQ water. (*B*) Three-dimensional representation of an AFM image of PEX lens capsule on glass using AAC mode in MilliQ water. (*C*) Two-dimensional representation of *A* (scale bar = 2 μm, z-scale = 20 nm). (*D*) Two-dimensional representation of *B* (scale bar = 2 μm, z-scale = 160 nm).

AFM imaging

Because lens capsule tissue has not been used previously for AFM analysis, imaging (using a nonfunctionalized tip) was carried out to optimize the technique of lens capsule mounting and to establish the relevant AFM parameters. Dehydration is often used in protein studies by AFM (46) and immunofluorescence (47). The surface of the normal lens capsule was not observed to be affected by dehydration (Fig. S1 and Fig. S2 in the Supporting Material for nondehydrated and rehydrated tissues, respectively). Hence drying of the lens capsule was used as this tissue adheres strongly to a clean glass substrate on dehydration. Even after rehydration in MilliQ water for $\geq$24 h, the tissue remained tightly attached to the substrate. AFM imaging with a nonfunctionalized tip using tapping mode of the rehydrated lens capsule tissue in MilliQ water allowed high resolution surface images of both control and PEX lens capsules (Fig. 1). The normal lens capsule surface was very soft, and many of the features were distorted or not resolved (Fig. 1, *A* and *C*). However, the sample topography was mostly smooth, with some fibers (1–10 nm high and 1–100 nm wide; Fig. S2 *A*) seen across the surface. These fiber like surface features were expected because the lens capsule is known to be composed predominantly of the fibrous basement membrane proteins collagen IV and laminin. These fiber proteins are networked with nidogen and perlecan (22) to form the basement membrane matrix. On the other

hand, the PEX lens capsules imaged in MilliQ water (Fig. 1, *B* and *D*) showed thicker and denser fibrous features of up to 5–55 nm high and 10–60 nm wide and in some cases many microns long (Fig. S2 *B*). On both normal and PEX capsules, granular fibers were occasionally observed, producing an effect similar to a string-of-pearls. This effect was pronounced in PEX images, as seen in Fig. 1, *B* and *D*. Some areas of the PEX capsule contained large aggregates of PEX material that we were unable to image, leading to a large variability in roughness values. Measurements for control lens capsules gave root mean-square roughness of 5–50 nm, whereas the PEX capsules were significantly rougher with values of 20–200 nm root mean-square. Hence, PEX images were acquired only on the areas of the capsule that were relatively less rough. PEX deposits are not uniformly distributed across the lens capsule and more deposits are seen in the peripheral area probably due to physical rubbing of the overlying iris.

EM images (22,48–51) of these tissues are incomparable in topography to the AFM images due to the completely different sample preparation and scales; however, they do confirm the flat nature of the tissue and the presence of a fibrous protein network. Topography AFM images obtained using nonfunctionalized tips showed that the lens capsule is a suitable tissue for TREC imaging, as areas of <50 nm root-mean square roughness can be found (7).

TREC imaging was applied successfully to both normal and PEX lens capsules in PBS buffer using anti-clusterin antibody functionalized AFM tips. PBS buffer has similar pH and ionic strength as the aqueous humor that bathes the lens capsule in vivo, and was therefore an ideal fluid for imaging conditions. Measurements were made in regions of interest of less than $5 \times 5\ \mu m^2$ at a scanning speed of =1 line/s to allow for molecular reorientation and binding. The tip oscillation amplitude was adjusted to allow the linker to stretch, but not unbind, to dampen the upper motion of the cantilever oscillation (this amplitude varied from 10 to 50 nm). As seen in Fig. 2 (*right panels*), the clusterin protein was detected on normal lens capsules. In recognition images (Figs. 2–4, *right panels*), dark spots represent amplitude dampening, and these spots correlate to topographical features in the same region of interest (Figs. 2–4, *left panels*). Recognition spots averaged 240 nm^2 in area representing small patches across the scanned regions, but did not seem to follow a specific distribution pattern. When compared to PEX capsule imaging, a difference in detection was observed; the dark spots corresponding to recognition (Fig. 3, *right panels*) formed in larger patches, showing an increased localization of protein. Furthermore, these patches were observed frequently in-between large fibers or around the junction of multiple fibers. The area of recognition spots averaged 1791 nm^2, with a general trend of having significantly larger areas of recognition than on normal lens capsules (Fig. 5). An independent *t*-test verified the statistical difference in the mean

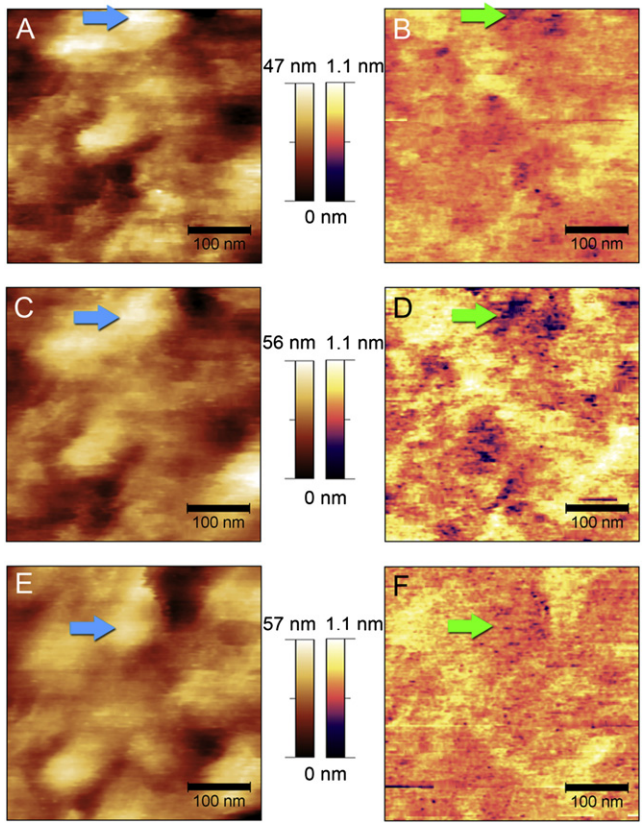

FIGURE 2 AFM images of normal lens capsule mounted on a glass slide using MAC mode in PBS. The left panels show topography images whereas the panels on the right show the corresponding TREC images. (*A* and *B*) Acquired with a tip oscillation amplitude of 22 nm. (*C* and *D*) Acquired with a tip oscillation amplitude of 33 nm. (*E* and *F*) Acquired with a tip oscillation amplitude of 44 nm. These amplitude variations are a method for confirming antibody specificity. The arrows point out corresponding topographical (*left*) and recognition (*right*). Scale bars = 100 nm.

recognition spot area between normal and PEX capsules ($t(1119) = -2.7$, two-tail $p < 0.007$), confirming the differences observed visually. However, it is important to note that to determine clinical significance, one would require a far larger number of samples (two normal and two PEX capsules were analyzed) than were used here. This can be the subject of a future clinical study. Furthermore, these results only reflect a difference in distribution of clusterin, and not a defined quantitative difference on the whole tissue.

Clusterin has been implicated in many protein aggregation diseases, such as Alzheimer's disease (52,53). Clusterin is a molecular chaperone, which is expressed in response to cellular stress and to inhibit apoptosis (53,54). It is downregulated in anterior segment tissues of PEX affected eyes and is an integral component of PEX deposits. Its presence in PEX material may be a response to cellular stress or an attempt by the natural system to clear abnormal aggregation of other proteins through its chaperone function. However, it may be a sign of the natural system being overwhelmed or of inhibition of the chaperone function of clusterin by

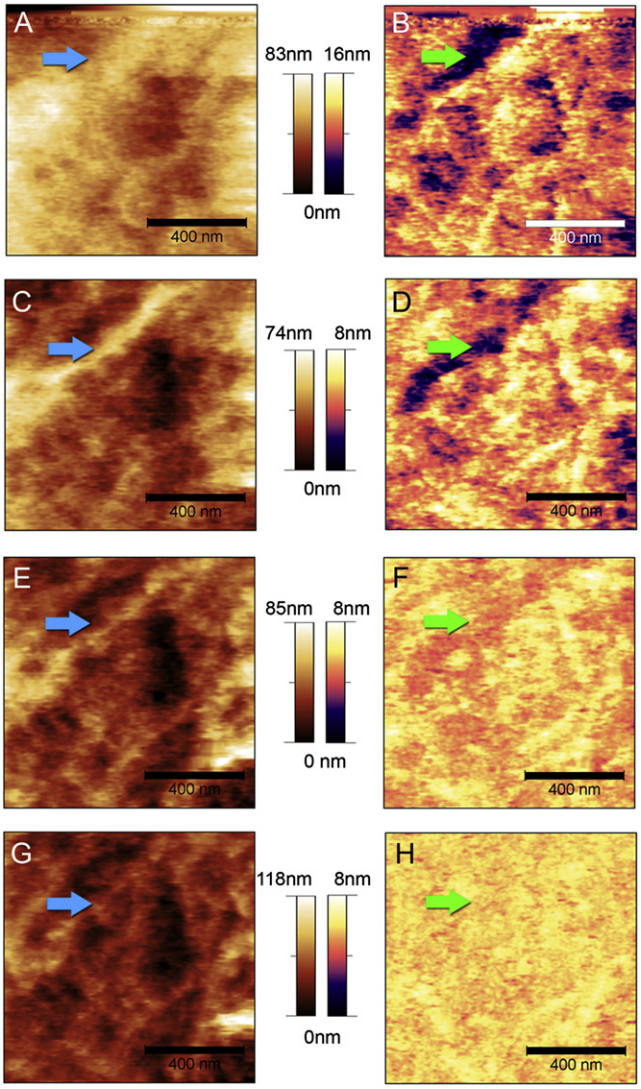

FIGURE 3 AFM images of PEX lens capsule on glass using MAC mode in PBS. On the left are topography images whereas the right side is the corresponding recognition images. (*A* and *B*) Acquired with a tip oscillation amplitude of 15 nm. (*C* and *D*) Acquired with a tip oscillation amplitude of 30 nm. (*E* and *F*) Acquired with a tip oscillation amplitude of 45 nm. (*G* and *H*) Acquired with a tip oscillation amplitude of 60 nm. These amplitude variations are a method for confirming antibody specificity. The arrows point out corresponding topographical (*left*) and recognition (*right*) features. Scale bars = 400 nm.

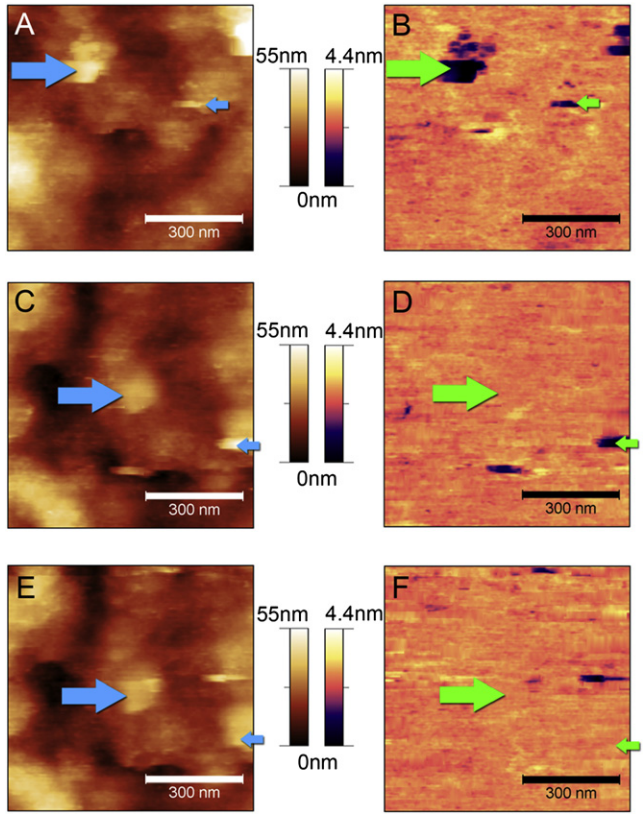

FIGURE 4 AFM images of normal lens capsule mounted on a glass slide using MAC mode in PBS with injection of anti-clusterin antibody (150 μg/mL) to block surface-bound clusterin. On the left are topography images whereas the right side is the corresponding recognition images. All images are acquired at a tip oscillation amplitude of 44 nm. (*A* and *B*) Acquired before addition of antibody. (*C* and *D*) Acquired 30 min after injection. (*E* and *F*) Acquired 50 min after injection. The arrows point out corresponding topographical (*left*) and recognition (*right*) features. Scale bars = 300 nm.

another molecule. Due to the enigmatic nature of the protein, however, its presence and function may actually be multifaceted including involvement in lipid movement, matrix stabilization, or other hitherto unknown functions (54).

Similar topography was observed using TREC imaging on both normal and PEX capsules as were seen previously in Fig. 1 using nonfunctionalized tips. Some difference in features in the topographical images acquired with TREC may appear broader than those acquired with a nonfunctionalized tip (7). This may be attributed to the length of the linker used to immobilize the antibody to the AFM tip, or to a tip broadening due to magnetic coating. One way of increasing image resolution is the use of a shorter linker. However, a shorter, less flexible linker may reduce or eliminate immunorecognition, depending on the antibody orientation. Alternatively, fixation has been reported to enhance TREC image resolution (17,18,55). Fixation was not attempted here because we were interested in studying the PEX aggregates in their native state.

Two control methods designed to remove the antibody binding event confirmed that recognition was specific for clusterin and not due to a topographical artifact. First, the introduction of free antibody into the solution, blocking surface-bound clusterin, resulted in a significant decrease in recognition as observed by the shrinking dark spots (*right panels*) in the TREC images of Fig. 4. This method of blocking is not ideal because it contaminates the system (7) and does not allow further TREC measurements on the same sample. For this reason it was only carried out once. Second, a more convenient control method was applied

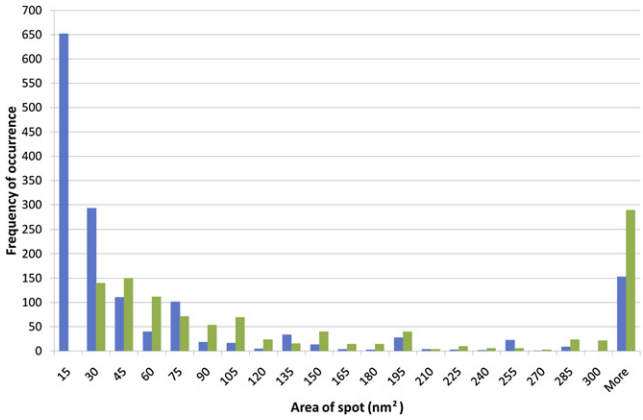

FIGURE 5 Frequency distribution histogram of TREC recognition spots observed across normal (■) and PEX (■) lens capsule samples measured as a unit of area (nm^2).

for every area analyzed. Recognition imaging is based on the use of the appropriate oscillation amplitude. If the linker is stretched too little at low oscillation amplitudes or, alternatively, if the receptor-ligand bond is broken at each oscillation cycle when using too large amplitudes, no pronounced and stable recognition events can be observed. We therefore increased the amplitude (while keeping the ratio of amplitude setpoint and free amplitude constant) to values above a threshold value to prove the specificity of the interactions. Too high amplitudes resulted in a breakage of the specific antibody-antigen bonds in the upper part of the oscillation (Fig. 2, *E* and *F*, and Fig. 3, *G* and *H*) (7); the disappearance of the recognition spots on increasing the oscillation amplitude shows clearly the specificity of the recognition. From force spectroscopy analysis, one would predict the threshold amplitude for this effect to be ~20 nm, the stretched length of the linker and the antibody. The experimentally determined threshold amplitude while imaging was higher, requiring an amplitude of up to 50 nm to remove recognition. This discrepancy may occur due to deformation of the lens capsule surface, contributing to the break-off length by acting as an additional spring. We also examined the amplitude error images (Fig. S3) because these indicate any feedback artifacts (known as topographical cross talk) that can occur due to inadequate signal decay. However, by using a frequency lower than the cantilever resonant frequency at the surface, topographical cross talk was minimized by allowing the topography signal to decay before the recognition signal is detected (7). We are confident, therefore, that the features seen in the TREC images are due to recognition events between the antibody on the tip and the sample.

Immunofluorescence labeling

Immunohistochemical studies carried out by Ovodenko et al. (26) confirm a significant presence of the clusterin protein in PEX aggregates on sections of PEX capsule. Such optical microscopy methods are limited in resolution and are not able to distinguish individual proteins or fibers in the PEX aggregates. However, these are established procedures for confirmation of presence of a protein and potential distribution patterns. Immunofluorescent labeling was carried out on whole lens capsules to further confirm the specificity of the antibody used, while also providing a technique to compare the TREC results. Initially, clusterin was detected in fresh normal lens capsules, as it is known to be present in the lens epithelial cells that remain attached to the lens side of the capsule after surgery. Propidium iodide counterstaining showed the nuclei, and clusterin was observed within the cells in the cytoplasm (Fig. S4). However, this protocol required permeabilization with methanol, which is not done in the AFM protocol, and may cause antibody trapping leading to nonspecific labeling. Therefore, further experiments were done without permeabilization.

The negative control samples (without a primary antibody) did not show significant fluorescence on the anterior side of the lens capsule suggesting the signal obtained with the anti-clusterin antibody to be specific. These samples were run with and without permeabilization, with no difference seen (R. Creasey, S. Sharma, J. Craig, and N. H. Voelcker, unpublished). Additional control labeling carried out with antibody against ZO-1, an intracellular protein, did not detect this protein on the anterior side of the capsule. Instead ZO-1 was seen on the lens side in the remnants of damaged lens epithelial cells (Fig. S5).

Clusterin was detected as a nearly homogenous layer across the anterior surface of the normal lens capsule (Fig. 6 *A*). It should be noted that in PEX the pathological material forms a layer across the lens capsule before it is clinically recognizable; as these controls come from cataract patients, there is a chance that the patient will develop PEX, but was not showing clinical symptoms at the time of lens

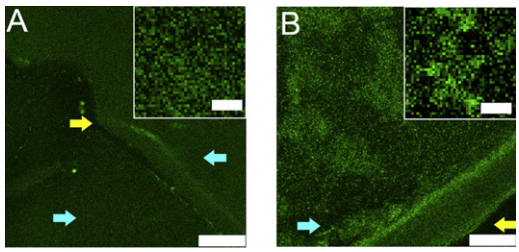

FIGURE 6 Confocal microscopy images of the anterior side of: (*A*) normal lens capsule (scale bar = 20 μm) with inset of digital zoom (scale bar = 500 nm); and (*B*) PEX lens capsule (scale bar = 20 μm) with inset of digital zoom (scale bar = 500 nm) immunolabeled with the anti-clusterin primary antibody and labeling detected with Alex Flour-488 conjugated anti-rabbit IgG secondary antibody. Image brightness curves adjusted for fluorescence visibility. Yellow arrows denote the edge of the tissue, and the cyan arrows denote the area of the image occupied by tissue. In *A*, this edge is due to the pinning procedure used during labeling, whereas *B* is the edge of the surgical cut of the lens capsule.

capsule collection. For this reason, several different patient capsules were used to confirm this clusterin layer across the normal anterior capsule, verifying that the clusterin is present in non-PEX cases. Clusterin showed a significantly stronger immunofluorescence signal on the anterior side of the PEX lens capsule, indicating higher expression is coincident with PEX deposits (Fig. 6 *B*). In particular, clusterin protein aggregates present were more prevalent in PEX cases. These results confirm that the PEX lens capsules have a different pattern of spatial clusterin distribution compared to normal capsules. The immunofluorescence data is consistent with TREC results where only small (<40 nm) areas of clusterin were present. However, this technique is clearly insufficient for molecular topographical studies. TREC images obtained contain 512 points/μm, whereas fluorescence images contained only 40 points/μm, and are also unable to show topography of PEX deposits.

In terms of PEX investigations, a further observation from these immunofluorescence data is that the clusterin does not appear to be permeating the lens capsule from the lens epithelial cells in normal (Fig. S4) or diseased capsules (R. Creasey, S. Sharma, J. Craig, and N. H. Voelcker, unpublished). It is known to be expressed from these cells; hence in this circumstance clusterin may be deposited from the aqueous humor. This may be an important piece of the PEX pathophysiological puzzle.

CONCLUSIONS

To our knowledge, the AFM recognition imaging technique TREC was used for the first time in this study to detect a protein on a human tissue sample. No fixation or processing of the tissue was applied. We investigated the pattern of apolipoprotein clusterin in the human lens capsule associated with the preglaucoma condition PEX. After proving the specificity of clusterin to anti-clusterin antibody binding by force spectroscopy, the clusterin protein was shown to be present on the surface of lens capsules using TREC and immunofluorescence. It was observed by both methods that clusterin aggregation patterns differed between normal and PEX lens capsules. This distribution pattern is thought to occur due to the aggregation of misfolded proteins in the PEX disease, leading to a chaperone response by the clusterin protein. Further investigations are warranted to confirm the pathological implications. We believe, however, that this study demonstrates successfully the feasibility of TREC imaging of biological tissues, and may be used to analyze protein aggregates in a physiological environment.

Investigation of fixed tissue sections may also be conducive to TREC imaging that would expand the scope of this approach to the study of other diseases such as neurodegenerative disorders or cancer. The possibilities of TREC imaging are far-reaching and go beyond the exploration of proteins implicated in diseases. For example, this approach can be applied to the characterization of protein or tissue interactions with synthetic biomaterials. Likewise, physiological processes such as the formation of new basement membranes can be explored. These applications deserve further investigation given our successful proof-of-principle.

SUPPORTING MATERIAL

Seven figures are available at http://www.biophysj.org/biophysj/supplemental/S0006-3495(10)00787-3.

We thank Dr. Linda Wildling, DI. Barbara Mayer, Dr. Rong Zhu, Alpana Dave, and DI. Markus Kastner for their technical assistance.

This study was supported by the National Health and Medical Research Council, Australia and by the European Community 7th framework program. R.C. was recipient of travel scholarships from the Fluorescence Applications for Biological Life Sciences, the Australian Society for Biomaterials and Tissue Engineering, and Flinders University. J.E.C. is recipient of National Health and Medical Research Council practitioner fellowship. A.E. is recipient of EC project "Single Molecule Workstation" 213717.

REFERENCES

1. Binnig, G., C. F. Quate, and C. Gerber. 1986. Atomic force microscope. *Phys. Rev. Lett.* 56:930–933.
2. Martin, Y., and H. K. Wickramasinghe. 1987. Magnetic imaging by force microscopy with 1000-A resolution. *Appl. Phys. Lett.* 50: 1455–1457.
3. Morris, V. J., A. R. Kirby, and A. P. Gunning. 2004. Atomic Force Microscopy for Biologists. Imperial College Press, London, UK.
4. Hansma, H. G., and J. H. Hoh. 1994. Biomolecular imaging with the atomic force microscope. *Annu. Rev. Biophys. Biomol. Struct.* 23: 115–139.
5. Stroh, C. M., A. Ebner, …, P. Hinterdorfer. 2004. Simultaneous topography and recognition imaging using force microscopy. *Biophys. J.* 87:1981–1990.
6. Johnson, W. T., G. Kada, …, P. Hinterdorfer. 2005. Simultaneous topography and recognition mapping with PicoTREC: a powerful new technology that can be used to map nanometer-scale molecular binding sites on a variety of surfaces. In NSTI-Nanotech 2005. www.nsti.org. 679–682.
7. Preiner, J., A. Ebner, …, P. Hinterdorfer. 2009. Simultaneous topography and recognition imaging: physical aspects and optimal imaging conditions. *Nanotechnology.* 20:215103.
8. Hinterdorfer, P., W. Baumgartner, …, H. Schindler. 1996. Detection and localization of individual antibody-antigen recognition events by atomic force microscopy. *Proc. Natl. Acad. Sci. USA.* 93:3477–3481.
9. Hinterdorfer, P., and Y. F. Dufrêne. 2006. Detection and localization of single molecular recognition events using atomic force microscopy. *Nat. Methods.* 3:347–355.
10. Ebner, A., F. Kienberger, …, P. Hinterdorfer. 2005. Localization of single avidin-biotin interactions using simultaneous topography and molecular recognition imaging. *ChemPhysChem.* 6:897–900.
11. Tang, J., A. Ebner, …, P. Hinterdorfer. 2008. Recognition imaging and highly ordered molecular templating of bacterial S-layer nano arrays containing affinity-tags. *Nano Lett.* 8:4312–4319.
12. Ebner, A., L. Wildling, …, H. Gruber. 2008. Functionalization of probe tips and supports for single-molecule recognition force microscopy. *Top. Curr. Chem.* 285:29–76.
13. Preiner, J., N. S. Losilla, …, P. Hinterdorfer. 2009. Imaging and detection of single molecule recognition events on organic semiconductor surfaces. *Nano Lett.* 9:571–575.
14. Reference deleted in proof.

15. Stroh, C., H. Wang, …, P. Hinterdorfer. 2004. Single-molecule recognition imaging microscopy. *Proc. Natl. Acad. Sci. USA.* 101:12503–12507.

16. Ebner, A., D. Nikova, …, H. Schillers. 2008. Determination of CFTR densities in erythrocyte plasma membranes using recognition imaging. *Nanotechnology.* 19:384017.

17. Chtcheglova, L. A., J. Waschke, …, P. Hinterdorfer. 2007. Nano-scale dynamic recognition imaging on vascular endothelial cells. *Biophys. J.* 93:L11–L13.

18. Chtcheglova, L. A., F. Atalar, …, P. Hinterdorfer. 2008. Localization of the ergtoxin-1 receptors on the voltage sensing domain of hERG K^+ channel by AFM recognition imaging. *Pflugers Arch.* 456:247–254.

19. Chen, P. P., H. T. Dong, …, D. Han. 2009. Application of atomic force microscopy to living samples from cells to fresh tissues. *Chin. Sci. Bull.* 54:2410–2415.

20. Meller, D., K. Peters, and K. Meller. 1997. Human cornea and sclera studied by atomic force microscopy. *Cell Tissue Res.* 288:111–118.

21. Buzhynskyy, N., J. F. Girmens, …, S. Scheuring. 2007. Human cataract lens membrane at subnanometer resolution. *J. Mol. Biol.* 374:162–169.

22. Danysh, B. P., and M. K. Duncan. 2009. The lens capsule. *Exp. Eye Res.* 88:151–164.

23. Dvorak-Theobald, G. 1953. Pseudoexfoliation of the lens capsule: relation to true exfoliation of the lens capsule as reported in the literature, and role in the production of glaucoma capsulocuticulare. *Trans. Am. Ophthalmol. Soc.* 51:385–407.

24. Lee, R. K. 2008. The molecular pathophysiology of pseudoexfoliation glaucoma. *Curr. Opin. Ophthalmol.* 19:95–101.

25. Johnson, M. 2006. 'What controls aqueous humour outflow resistance?'. *Exp. Eye Res.* 82:545–557.

26. Ovodenko, B., A. Rostagno, …, R. Ritch. 2007. Proteomic analysis of exfoliation deposits. *Invest. Ophthalmol. Vis. Sci.* 48:1447–1457.

27. Sharma, S., T. Chataway, …, J. E. Craig. 2009. Identification of *LOXL1* protein and Apolipoprotein E as components of surgically isolated pseudoexfoliation material by direct mass spectrometry. *Exp. Eye Res.* 89:479–485.

28. Liu, X. Q., Y. Zhao, …, T. Li. 2004. Elastic fiber homeostasis requires lysyl oxidase-like 1 protein. *Nat. Genet.* 36:178–182.

29. Drolsum, L., A. Ringvold, and B. Nicolaissen. 2007. Cataract and glaucoma surgery in pseudoexfoliation syndrome: a review. *Acta Ophthalmol. Scand.* 85:810–821.

30. Ringvold, A., G. Husby, and S. Pettersen. 1989. Electrophoretic study of proteins associated with pseudo-exfoliation syndrome. *Acta Ophthalmol. (Copenh.).* 67:724–726.

31. Burdon, K. P., S. Sharma, …, J. E. Craig. 2008. Genetic analysis of the clusterin gene in pseudoexfoliation syndrome. *Mol. Vis.* 14:1727–1736.

32. Zenkel, M., E. Pöschl, …, U. Schlötzer-Schrehardt. 2005. Differential gene expression in pseudoexfoliation syndrome. *Invest. Ophthalmol. Vis. Sci.* 46:3742–3752.

33. Krumbiegel, M., F. Pasutto, …, A. Reis. 2009. Exploring functional candidate genes for genetic association in german patients with pseudoexfoliation syndrome and pseudoexfoliation glaucoma. *Invest. Ophthalmol. Vis. Sci.* 50:2796–2801.

34. Thorleifsson, G., K. P. Magnusson, …, K. Stefansson. 2007. Common sequence variants in the *LOXL1* gene confer susceptibility to exfoliation glaucoma. *Science.* 317:1397–1400.

35. Schlötzer-Schrehardt, U. 2009. Molecular pathology of pseudoexfoliation syndrome/glaucoma—new insights from *LOXL1* gene associations. *Exp. Eye Res.* 88:776–785.

36. Hewitt, A. W., S. Sharma, …, J. E. Craig. 2008. Ancestral *LOXL1* variants are associated with pseudoexfoliation in Caucasian Australians but with markedly lower penetrance than in Nordic people. *Hum. Mol. Genet.* 17:710–716.

37. Schlötzer-Schrehardt, U., K. von der Mark, …, G. O. Naumann. 1997. Increased extracellular deposition of fibrillin-containing fibrils in pseudoexfoliation syndrome. *Invest. Ophthalmol. Vis. Sci.* 38:970–984.

38. Schlötzer-Schrehardt, U., and G. O. Naumann. 2006. Ocular and systemic pseudoexfoliation syndrome. *Am. J. Ophthalmol.* 141:921–937.

39. Ebner, A., L. Wildling, …, H. J. Gruber. 2007. A new, simple method for linking of antibodies to atomic force microscopy tips. *Bioconjug. Chem.* 18:1176–1184.

40. Ebner, A., P. Hinterdorfer, and H. J. Gruber. 2007. Comparison of different amino functionalization strategies for attachment of single antibodies to AFM cantilevers. *Ultramicroscopy.* 107:922–927.

41. Riener, C. K., C. M. Stroh, …, H. J. Gruber. 2003. Simple test system for single molecule recognition force microscopy. *Anal. Chim. Acta.* 479:59–75.

42. Sader, J. E., J. W. M. Chon, and P. Mulvaney. 1999. Calibration of rectangular atomic force microscope cantilevers. *Rev. Sci. Instrum.* 70:3967–3969.

43. Hutter, J. L., and J. Bechhoefer. 1993. Calibration of atomic-force microscope tips. *Rev. Sci. Instrum.* 64:1868–1873.

44. Rankl, C., F. Kienberger, H. Gruber, D. Blaas, and P. Hinterdorfer. 2007. Accuracy estimation in force spectroscopy experiments. *Jpn. J. Appl. Phys.* 46:5536–5539.

45. Lee, C. K., Y. M. Wang, …, S. Lin. 2007. Atomic force microscopy: determination of unbinding force, off rate and energy barrier for protein-ligand interaction. *Micron.* 38:446–461.

46. Pountney, D. L., R. Lowe, …, W. P. Gai. 2004. Annular alpha-synuclein species from purified multiple system atrophy inclusions. *J. Neurochem.* 90:502–512.

47. Zenkel, M., F. E. Kruse, …, U. Schlötzer-Schrehardt. 2006. Clusterin deficiency in eyes with pseudoexfoliation syndrome may be implicated in the aggregation and deposition of pseudoexfoliative material. *Invest. Ophthalmol. Vis. Sci.* 47:1982–1990.

48. Parekh, P., W. R. Green, …, E. K. Akpek. 2008. Electron microscopic investigation of the lens capsule and conjunctival tissues in individuals with clinically unilateral pseudoexfoliation syndrome. *Ophthalmology.* 115:614–619, e2.

49. Takei, Y., and K. Mizuno. 1978. Electron-microscopic study of pseudoexfoliation of the lens capsule. *Albrecht Von Graefes Arch. Klin. Exp. Ophthalmol.* 205:213–220.

50. Vesti, E., and T. Kivel ä. 2000. Exfoliation syndrome and exfoliation glaucoma. *Prog. Retin. Eye Res.* 19:345–368.

51. Winkler, J., H. Lünsdorf, …, H. Laqua. 2001. Immunohistochemical and charge-specific localization of anionic constituents in pseudoexfoliation deposits on the central anterior lens capsule from individuals with pseudoexfoliation syndrome. *Graefes Arch. Clin. Exp. Ophthalmol.* 239:952–960.

52. Lambert, J.-C., S. Heath, …, P. Amouyel, European Alzheimer's Disease Initiative Investigators. 2009. Genome-wide association study identifies variants at CLU and CR1 associated with Alzheimer's disease. *Nat. Genet.* 41:1094–1099.

53. Calero, M., A. Rostagno, …, J. Ghiso. 2000. Apolipoprotein J (clusterin) and Alzheimer's disease. *Microsc. Res. Tech.* 50:305–315.

54. Jones, S. E., and C. Jomary. 2002. Clusterin. *Int. J. Biochem. Cell Biol.* 34:427–431.

55. Baumgartner, W., P. Hinterdorfer, …, D. Drenckhahn. 2000. Cadherin interaction probed by atomic force microscopy. *Proc. Natl. Acad. Sci. USA.* 97:4005–4010.